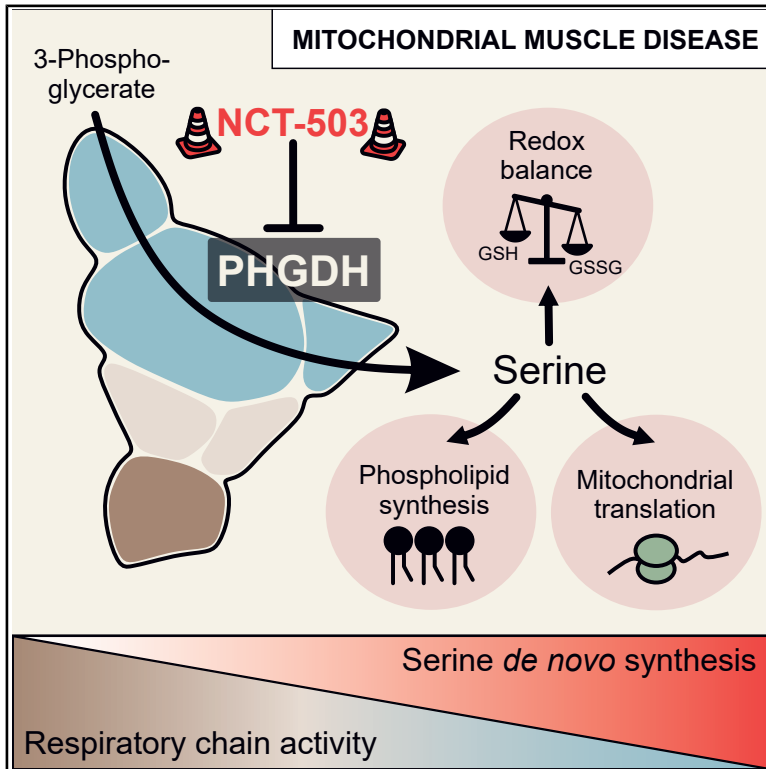


De novo serine biosynthesis is protective in mitochondrial disease

Graphical abstract



Authors

Christopher B. Jackson, Anastasiia Marmyleva, Geoffray Monteouis, ..., Thomas Langer, Christopher J. Carroll, Anu Suomalainen

Correspondence

christopher.jackson@helsinki.fi (C.B.J.), anu.wartiovaara@helsinki.fi (A.S.)

In brief

Jackson et al. show that serine becomes an essential amino acid in mitochondrial muscle disease, delaying disease progression. Blocking local biosynthesis of serine challenges cellular phospholipid homeostasis and redox balance in the context of disease but is not harmful to healthy physiology.

Highlights

- Serine becomes an essential amino acid in mitochondrial translation defects
- Blocking *de novo* serine biosynthesis promotes progression of mitochondrial disease
- *De novo* serine biosynthesis maintains phospholipid homeostasis upon mitochondrial insult
- Serine biosynthesis sustains redox balance and mitochondrial translation in disease



Article

De novo serine biosynthesis is protective in mitochondrial disease

Christopher B. Jackson,^{1,2,10,11,*} Anastasiia Marmyleva,^{1,10} Geoffray Monteuis,² Ryan Awadhpersad,² Takayuki Mito,¹ Nicola Zamboni,³ Takashi Tatsuta,⁴ Amy E. Vincent,⁵ Liya Wang,⁶ Nahid A. Khan,¹ Thomas Langer,⁴ Christopher J. Carroll,^{1,7} and Anu Suomalainen^{1,8,9,*}

¹Research Programs Unit, Stem Cells and Metabolism, University of Helsinki, 00290 Helsinki, Finland

²Department of Biochemistry and Developmental Biology, University of Helsinki, 00290 Helsinki, Finland

³Institute of Molecular Systems Biology, Department of Biology, ETH Zurich, 8093 Zurich, Switzerland

⁴Max Planck Institute for Aging, 50931 Cologne, Germany

⁵Wellcome Centre for Mitochondrial Research, Translational and Clinical Research Institute, Faculty of Medical Sciences, Newcastle University, NE2 4HH Newcastle upon Tyne, UK

⁶Department of Animal Biosciences, Swedish University of Agricultural Sciences, 75007 Uppsala, Sweden

⁷Cardiovascular and Genomics Research Institute, School of Health and Medical Sciences, City St. George's, University of London, SW17 0RE London, UK

⁸HUS Diagnostic Center, Helsinki University Hospital, 00290 Helsinki, Finland

⁹HiLife, University of Helsinki, 00290 Helsinki, Finland

¹⁰These authors contributed equally

¹¹Lead contact

*Correspondence: christopher.jackson@helsinki.fi (C.B.J.), anu.wartiovaara@helsinki.fi (A.S.)

<https://doi.org/10.1016/j.celrep.2025.115710>

SUMMARY

The importance of serine as a metabolic regulator is well known for tumors and is also gaining attention in degenerative diseases. Recent data indicate that *de novo* serine biosynthesis is an integral component of the metabolic response to mitochondrial disease, but the roles of the response have remained unknown. Here, we report that glucose-driven *de novo* serine biosynthesis maintains metabolic homeostasis in energetic stress. Pharmacological inhibition of the rate-limiting enzyme, phosphoglycerate dehydrogenase (PHGDH), aggravated mitochondrial muscle disease, suppressed oxidative phosphorylation and mitochondrial translation, altered whole-cell lipid profiles, and enhanced the mitochondrial integrated stress response (ISR^{mt}) *in vivo* in skeletal muscle and in cultured cells. Our evidence indicates that *de novo* serine biosynthesis is essential to maintain mitochondrial respiration, redox balance, and cellular lipid homeostasis in skeletal muscle with mitochondrial dysfunction. Our evidence implies that interventions activating *de novo* serine synthesis may protect against mitochondrial failure in skeletal muscle.

INTRODUCTION

Mitochondria are organelles that function at the crossroads of both catabolic and anabolic processes of cellular metabolism.¹ The central catabolic function of mitochondria is oxidative breakdown of nutrients to produce ATP. This function is preferential when nutrient availability is low. Upon high nutrient availability, cytoplasmic glycolysis is upregulated for ATP production, with mitochondria enhancing production of metabolites, amino acids, and cofactors for anabolic growth.² The biosynthetic pathways are highly tissue and cell type specific, making tissues differently sensitive to stress and disease-linked challenges. Therefore, it is not surprising that defects in mitochondrial function cause an exceptionally broad spectrum of human disorders, ranging from neurodegeneration to heart, muscle, and endocrine disorders.^{1,3} The molecular details of disease-related metabolic remodeling and the relevance to disease progression are only starting to be revealed.

Mitochondrial myopathy (MM) is a common form of mitochondrial diseases, typically caused by mutations in genes encoding proteins involved in mitochondrial DNA (mtDNA) expression, replication, or translation.³ These defects induce complex stress responses (mitochondrial integrated stress response [ISR^{mt}]) involving remodeling of cellular anabolic metabolism, including the folate cycle, the methyl cycle, nucleotide and glutathione synthesis, as well as production and secretion of the metabolites FGF21 and GDF15 in mice and cell cultures,^{4–9} and are conserved in human patients.^{10,11} Recent data indicate that ISR^{mt} occurs stagewise, first involving transcriptional activation of ATF5, metabolites, and the mitochondrial folate cycle, followed by a second stage of upregulated *de novo* serine synthesis and mTORC1 activation.^{4,6,12} These previous data have indicated that primary mitochondrial defects cause a remarkable cell-autonomous remodeling of cellular metabolism. Furthermore, the non-cell-autonomous ISR^{mt} response, which occurs via secretion of the metabolites GDF15 and FGF21,



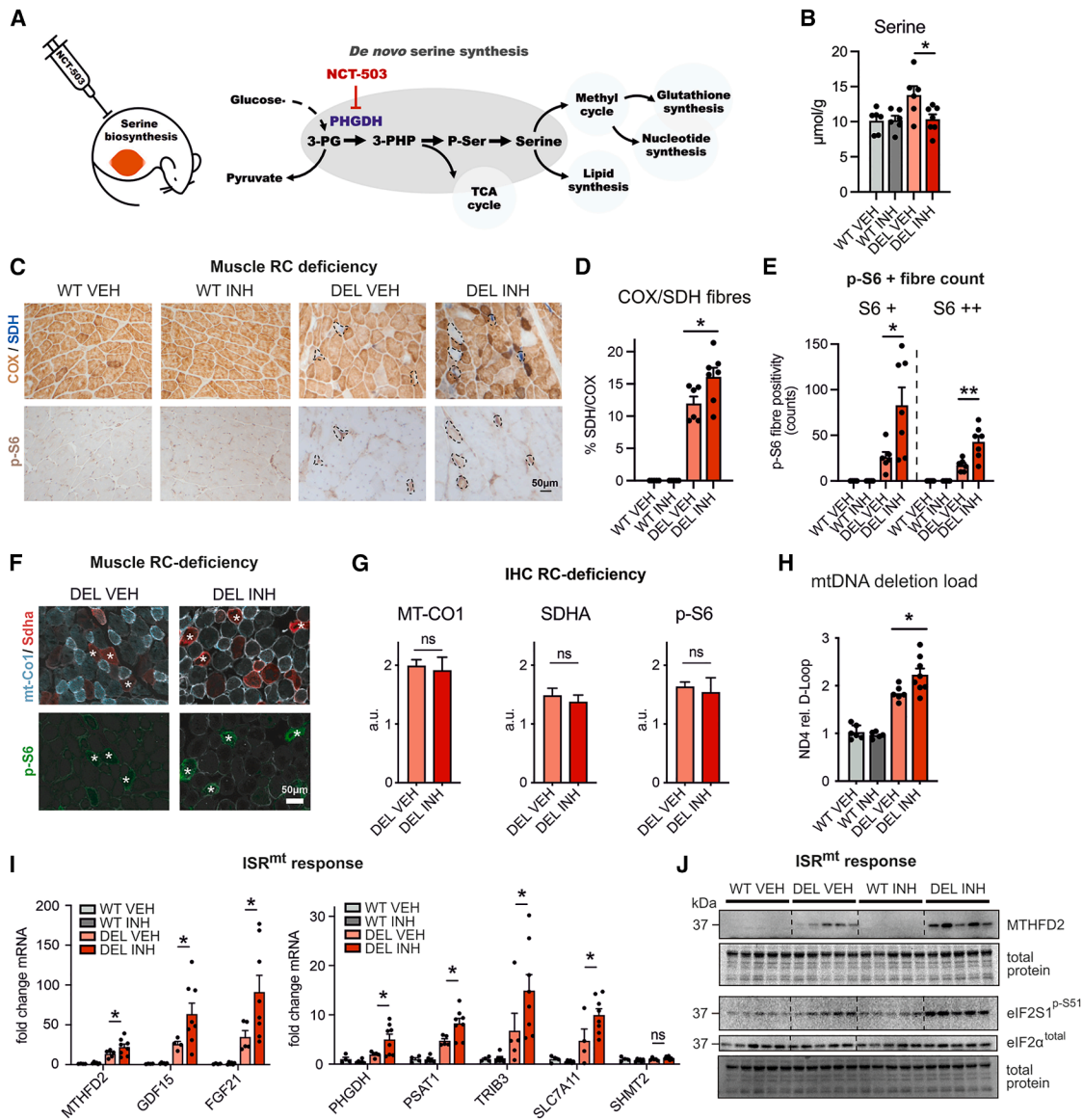


Figure 1. Systemic NCT-503 administration effectively inhibits dnSB in MM

(A) Serine inhibition treatment trial and *de novo* serine synthesis-related cellular pathways.

(B) Serine amount upon PHGDH inhibition. NCT-503 administration for 30 days; targeted metabolomics of skeletal muscle (WT VEH *n* = 6, DEL VEH *n* = 6, WT INH *n* = 6, DEL INH *n* = 7).

(C) Effects of PHGDH inhibition on RC deficiency. Shown is histochemical analysis of combined cytochrome c oxidase (COX) and succinate dehydrogenase (SDH) activity. Brown fibers indicate high COX activity and translucent ones low COX activity. Blue fibers indicate high SDH activity and mitochondrial proliferation and translucent ones low SDH activity. Bottom: immunohistochemical detection of the mTORC1 downstream target phosphorylated ribosomal S6 (p-S6). Images represent sequential frozen sections, and black circles match fibers in subsequent sections. Scale bar: 50 µm.

(D) Quantification of RC deficiency in skeletal muscle from (C): percentage of COX- and SDH+ fibers in treated and untreated Deletors (DEL VEH *n* = 6, DEL INH *n* = 7).

(E) Amount of strong (+) and very strong (++) p-S6 fibers in treated and untreated Deletors (DEL VEH *n* = 6, DEL INH *n* = 7).

(F) Immunofluorescence imaging of Deletor muscle cryosections probed for mitochondrially encoded protein (MT-CO1, light blue), mitochondrial mass (Sdha, red), and a myofiber membrane marker (Laminin, white). Bottom: immunofluorescence for p-S6 (green). Asterisks: COX- /SDH+ or p-S6+ fibers. Scale bar: 50 µm.

(G) Quantification of total immunofluorescence of grouped VEH and INH animals from (F). INH animals show unchanged MT-CO1, SDHA, and p-S6 levels. a.u., arbitrary units.

(H) MtDNA deletion load; qPCR (ratio of deleted ND4/intact D Loop) (WT VEH *n* = 6, DEL VEH *n* = 6, WT INH *n* = 6, DEL INH *n* = 8). Results were normalized to untreated WT mice.

(I) Transcriptional induction of ISR^{mt} markers. qPCR; relative to β-actin (WT VEH *n* = 6, DEL VEH *n* = 6, WT INH *n* = 6, DEL INH *n* = 8).

(legend continued on next page)

systematically modifies fat and glucose metabolism.^{4,13} However, whether ISR^{mt} promotes or protects from disease progression *in vivo*, and whether its components can be therapeutic targets, remains unclear.

De novo serine biosynthesis (dnSB) is an integral upregulated component of ISR^{mt} in both postmitotic and cultured cells^{4,6,8} as well as a key component to promote anabolic growth in cancer cells.^{14–16} The regulatory enzyme of dnSB is phosphoglycerate dehydrogenase (PHGDH; EC1.1.1.95), catalyzing the first and rate-limiting step of the three-step process that bifurcates glucose flux from glycolysis to dnSB.^{8,14,17,18} In addition to its function as a proteinogenic amino acid in the muscle, serine donates its one-carbon (1C) units via the folate cycle for nucleotide synthesis and supports glutathione (GSH) and heme synthesis and nicotinamide adenine dinucleotide phosphate synthesis, making serine a major contributor to the cellular redox pool and pentose phosphate pathway.^{18–20} Furthermore, serine supports membrane phospholipid synthesis by providing the head group of phosphatidylserines and serves as a substrate for sphingolipid synthesis.²¹

The reason why serine needs to be synthesized as part of a metabolic stress response and which of its functions are required upon metabolic stress in different cell types are unknown. Here, we studied dnSB in Deletor mice, a mouse model that manifests with similar findings as patients with adult-onset MM: slowly progressive mtDNA mutagenesis and respiratory chain deficiency.²² In these mice, dnSB induction is a key component of their disease.^{4,13} We report here the consequences of inhibited PHGDH activity in Deletor mice and in cultured cells with mitochondrial dysfunction. We find that dnSB is critical for maintenance of cellular metabolic homeostasis and viability in mitochondrial stress and disease.

RESULTS

Inhibition of dnSB aggravates mitochondrial pathology

To test the importance of dnSB for mitochondrial disease progression, we systematically treated Deletor mice, which ubiquitously express a homologous dominant patient mutation in the mitochondrial helicase *twinkle* (*Twinkle*^{dup353–365}),²² and wild-type (WT) mice with vehicle or NCT-503, an inhibitor of PHGDH, the rate-limiting dnSB enzyme (Figure 1A,¹⁵). Thirty days of daily intraperitoneal injections did not have visible effects on mouse well-being or body weight, indicating no apparent systemic toxicity for NCT-503, as also reported before (Figure S1A).¹⁵

In the Deletor *quadriceps femoris* muscle, the inhibitor efficiently reduced serine levels to the level of WT mice (Figures 1B and S1B) while not affecting the amounts in the WT muscle. These results indicate the efficacy of the drug *in vivo* and the specificity of PHGDH as a regulator of serine levels in mitochondrial disease. Analysis of respiratory chain enzyme activities indicated that PHGDH inhibition increased the number of respiratory chain (RC)-deficient fibers (cytochrome *c* oxidase deficient [COX negative] and elevated pathology-related succinate dehydrogenase

activity [SDH positive]) (Figures 1C and 1D) in the Deletor muscle with no effect on WT mice. However, COX and SDH protein amounts were not significantly altered (Figures 1F and 1G). NCT-503 treatment also increased the number of fibers with activated mTORC1 (mechanistic target of rapamycin complex 1; activity readout: phosphorylation of S6 [p-S6], a cytoplasmic ribosome component) (Figure 1E). In WT mice, we did not observe any COX- or p-S6-activated fibers in treated or untreated animals (Figures 1C–1E). In Deletors, the total mitochondrial mass in the skeletal muscle and the total fiber size were not significantly affected by the inhibitor treatment, and the proportion of fibers with central nuclei remained the same (Figures 1F and S1C), but mitochondria appeared distorted (Figure S1D). Also, multiple mtDNA deletion load increased (Figure 1H). The mtDNA content did not significantly increase in treated Deletors but showed elevated levels compared to WT mice (Figure S1E). These results show that *de novo* serine synthesis delays generation of mtDNA deletions and progression of mitochondrial pathology.

The transcriptional ISR^{mt} response components (*MTHFD2*, *GDF15*, *FGF21*, *PSAT1*, *TRIB3*, and *SLC7A11*) were further induced by the NCT-503 treatment compared to the vehicle (Figures 1I and S1F). *PHGDH* transcription was especially stimulated by the inhibition of PHGDH enzyme activity, suggesting a feedback mechanism (Figure 1I). We tested the effect of NCT-503 by treating an independent Deletor transgenic line (Deletor C-line), which has lower mutant *Twinkle* expression compared to control mice. The Deletor C-line showed a similar induction for PHGDH upon dnSB inhibition (Figure S1G). The induction of ISR^{mt} was also confirmed at the protein level (*MTHFD2*; Figure 1J). Eukaryotic translation initiation factor 2 subunit 1, a key component of the cytoplasmic integrated stress response, showed increased phosphorylation levels (Figures 1J and S1H), and the UPR^{mt} marker HSP70 was significantly increased at the protein level (Figures S1I and S1J). WT mice showed no changes in ISR^{mt} upon treatment, highlighting the specific role of dnSB in the context of disease (Figure 1I). Transcript analysis of muscle atrophy markers *MURF1* and *ATROGIN1* showed slightly increased expression after PHGDH inhibitor treatment in Deletor and WT mice (Figure S1K). However, the muscles expressed no histological signs of cell death. In addition, treatment in a control group of WT mice with and without inhibitor showed no impact on mitochondrial respiration in *quadriceps femoris* (QF) muscle (Figure S1L).

Altogether, these findings demonstrate vulnerability of muscles with mitochondrial dysfunction to restriction of serine biosynthesis.

Inhibition of PHGDH alters metabolic profile and lipid balance in MM

Next, we analyzed the muscle metabolome of healthy and diseased mouse muscle upon dnSB inhibition. Supervised principal-component analysis indicated separation of the Deletor metabolome from the WT, which was further altered by NCT-503 (Figure S2A). For the WT mice, the treatment had little effect

(J) Translational induction of the ISR^{mt} marker *MTHFD2* and phosphorylation status of eIF2 α . Immunoblot ($n = 5$ /group). Animals were 25 months old. Bars represent the group average and error bars SEM; individual animals or skeletal fibers are shown as dots. Statistical significance was determined using ANOVA. * $p \leq 0.05$, ** $p \leq 0.01$. *** $p \leq 0.001$. WT, wild type; DEL, Deletor; VEH, vehicle; INH, NCT-503; PHGDH, phosphoglycerate dehydrogenase.

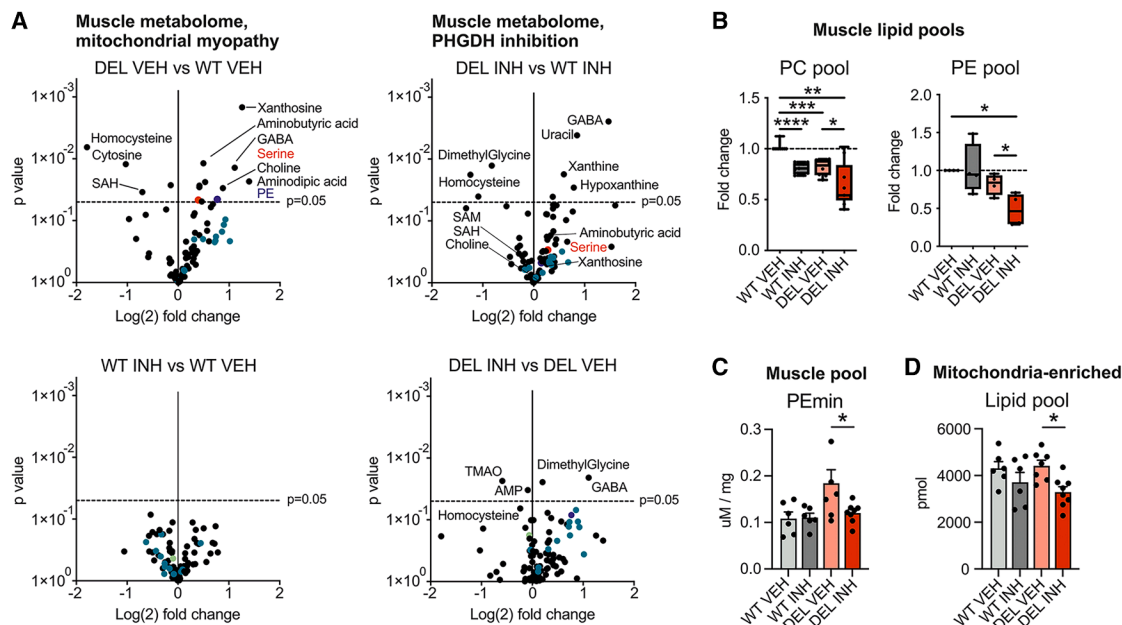


Figure 2. Serine biosynthesis inhibition increases hallmarks of MM and alters lipid balance

(A) Metabolomic analysis of skeletal muscle. Shown are volcano plots of Deletor and WT mice left untreated or treated with NCT-503. Dots represent individual metabolites. Green, acyl-carnitines; red, serine. WT VEH $n = 6$, DEL VEH $n = 6$, WT INH $n = 6$, DEL INH $n = 8$.

(B) Alteration of total PC and PE pools in whole muscle; untargeted metabolomics. Each dot represents the median value of all animals for a detected lipid species.

(C) PEmin level; targeted metabolomics of whole muscle (WT VEH $n = 5$, DEL VEH $n = 7$, WT INH $n = 6$, DEL INH $n = 8$).

(D) Total lipid content in the mitochondrion-enriched fraction from whole muscle (WT VEH $n = 6$, DEL VEH $n = 7$, WT INH $n = 6$, DEL INH $n = 8$).

Bars represent the group average and error bars SEM; individual animals are shown as dots. Statistical significance was assessed using ANOVA. * $p \leq 0.05$, ** $p \leq 0.01$, *** $p \leq 0.001$. PC, phosphatidylcholine; PE, phosphatidylethanolamine; PEmin, phosphoethanolamine.

(Figure 2A). NCT-503 significantly affected 1C metabolism (nucleotide and GSH synthesis, methyl cycle, and phospholipid pools), since serine contributes to it in various ways. The nucleotide synthesis intermediates xanthine and hypoxanthine accumulated in Deletor mice, and these were further increased by NCT-503 (Figure 2A). The highest and most significantly changed metabolite after inhibitor treatment in Deletors was gamma-aminobutyric acid, reported to accumulate if mitochondrial nucleoside salvage is deficient.²³ While we observed decreased levels of S-adenosylmethionine (SAM) and/or S-adenosyl-L-homocysteine (SAH) in Deletors (Figure 2A), the SAM/SAH ratio remained stable independent of genotype and treatments (Figure S2B). On the other hand, the ratio of oxidized to non-oxidized GSH was increased between Deletors compared to WT mice and non-significantly between treated and non-treated Deletors (Figure S2C). Apart from serine, the total level of non-essential amino acids was increased in Deletors compared to WT mice but decreased upon treatment (Figures S2D and S2E). In a separate analysis of total dNTP pools, dCTP was increased, while the metabolomics indicated decreased steady-state cytosine, potentially as a consequence of altered usage (Figure S2F). These results, together with the ISR^{mt} induction, supported the conclusion that dnSB is protective in mitochondrial disease *in vivo*.

The metabolomics analysis highlighted the importance of dnSB for phospholipid homeostasis. Intriguingly, in mitochondrion-enriched fractions, the phosphatidylethanolamine (PE) pool was

increased (Figures S2G and S2H), whereas in the total muscle pool it was low (Figure 2B). The total and mitochondrial phosphatidylcholine (PC) pools, however, were depleted by NCT-503 both in healthy and diseased mice (Figures 2B, S2G, and S2H). In inhibitor-treated Deletor muscle phosphoethanolamine levels were normalized (Figure 2C), while the total mitochondrial lipid pool was reduced in treated mice (Figure 2D). These data emphasize the necessity of dnSB for phospholipid homeostasis in skeletal muscle and especially in mitochondria. Cardiolipin (CL), specific for mitochondrial membranes, increased in amount after PHGDH inhibition in the Deletors, indicating a role of dnSB for CL homeostasis in mitochondria (Figures S2G and S2H). Next, we asked whether the changed mitochondrial lipid composition affected processing of OPA1, a GTPase controlling mitochondrial membrane dynamics, which binds to CL and is activated in the inner mitochondrial membrane by proteolytic cleavage. However, OPA1 processing was unaffected in whole-skeletal-muscle homogenates of all our mouse groups (Figure S2I).

To investigate whether dnSB is a response to potential intramitochondrial serine availability, we assessed the steady-state level of the mitochondrial serine transporter SFXN1, which was increased 4-fold in treated Deletors compared to wild type and trended towards increase in treated wild-type mice as well (Figure S2J).

Together, these data show a remarkable remodeling of serine-dependent homeostasis in mitochondrial disease. The evidence

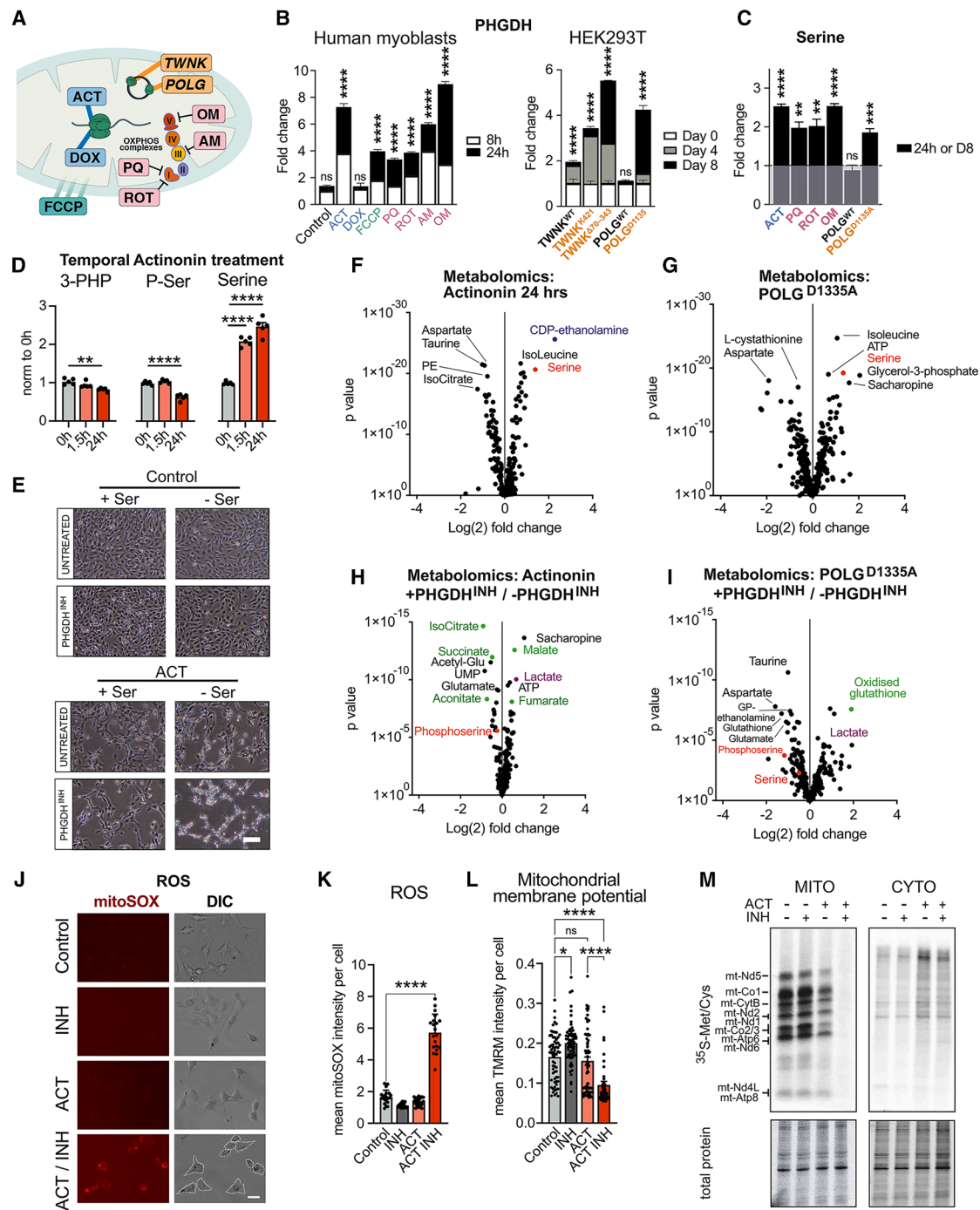


Figure 3. Serine availability and *de novo* serine synthesis affect cell fitness dependent on mitochondrial dysfunction

(A) Cellular models of mitochondrial dysfunction. Shown are compounds acting on the mitochondrial ribosome (ACT and DOX), a protonophore acting on membrane potential (FCCP, green), compounds directly affecting the RC (PQ, ROT, AM, and OM, red), and genetic models of dysfunction by mutant over-expression (TWNK and POLG). Cells were grown in serine-containing medium.

(B) PHGDH transcript levels. Left: human myoblasts with the indicated treatment for 8 and 24 h. Right: HEK293T cells with overexpressed POLG, WT, or mutant TWNK for 4–8 days. Normalization against corresponding non-treated or uninduced controls. Error bars represent triplicate measurement (SD).

(C) Serine levels in cells treated either for 24 h with mitochondrial toxins or with 8-day POLG mutant overexpression. Data were normalized to the respective untreated controls. Values were determined from untargeted metabolomics. Error bars represent SD of biological quintuplicates.

(D) Relative expression of serine *de novo* synthesis metabolites (3-phosphohydroxypyruvate [3-PHP], 3-phosphoserine [p-Ser], and serine) upon temporal actinonin treatment. Untargeted metabolomics. Intensities were calculated from biological quintuplicates. Error bars represent SD.

(legend continued on next page)

indicates that phospholipid homeostasis is dependent on dnSB, especially in mitochondrial disease, as PE and CL were high in mitochondria, while the total cellular pools for PE were low (Figures S2G and S2H). Furthermore, mitochondrial serine uptake and translation appear to be supported by dnSB. The data suggest that dnSB is a protective response in mitochondrial disease progression, fueling mitochondrial translation capacity, and alters phospholipid homeostasis.

De novo serine synthesis is an early response to various mitochondrial stresses

To further understand the relevance of *de novo* serine synthesis in different kinds of mitochondrial insults, we tested temporal treatments of cultured cells with various mitochondrial toxins (Figure 3A): (1) paraquat, causing oxidative stress in the mitochondrial matrix; (2) rotenone, a complex I inhibitor; (3) oligomycin, an F_0F_1 -ATPase (complex V) inhibitor; (4) antimycin, a complex III inhibitor; (5) actinonin and doxycycline, two mitochondrial translation inhibitors; and (6) p-trifluoro-methoxyphenyl hydrazone (FCCP), an oxidative phosphorylation (OXPHOS) uncoupler. We also induced mtDNA depletion stress by overexpression of mutants of the mitochondrial helicase Twinkle (TWNK) and polymerase gamma (POLG), which lead to a progressive RC deficiency (Figure S3A). PHGDH expression (Figure 3B) and increased serine levels (Figure 3C) responded consistently to the different inhibitors of mitochondrial functions. Upstream regulators of ISR^{mt}, ATF3-ATF5, were induced after different stressors in cultured myoblasts; ATF3 was especially highly induced upon oxidative stress (paraquat and rotenone), while all ATFs responded to actinonin-induced mitochondrial translation stress (Figure S3B). These results indicate that dnSB induction is a key component of stress responses to different mitochondrial inhibitors and genetic insults of the mtDNA replisome.

We then asked whether dnSB is an early or late component in ISR^{mt} progression in cultured cells (primary diploid human myoblasts) and chose to use actinonin as a stressor for the mtDNA expression system, also sharing the stress type closely in the Deleter mouse muscle.²⁴ Untargeted metabolomics analysis of actinonin-treated cells revealed a time-dependent decrease in PSAT1-dependent phosphoserine, while serine was increased

after 1.5 h exposure (Figure 3D). Similar to the results from skeletal muscle, the phospholipid pools (PE and PC species) decreased after 16 h of exposure, while the PE precursor started to accumulate at that time (Figures S3C and S3D). The ultrastructure of the inhibitor-treated cells showed complete loss of cristae with the appearance of myelinosome-like membranous lipid aggregates (Figure S3E). Furthermore, short-term exposure to actinonin resulted in a shift to increased p-S6 levels, a target of mTORC1, with a similar timeline as that of nucleotide metabolism and aspartate increase. The decline of mTORC1 was accompanied by an increase in ATF4 activation (Figure S3F). These results demonstrate that mitochondrial translation stress involves dnSB as an early response.

Serine can be derived from both exogenous and endogenous sources.^{14,25} We tested the effect of dnSB upon mitochondrial dysfunction by eliminating the exogenous source by pre-culturing the cells in serine-free medium for 24 h. In healthy cells, a continued 24-h treatment with NCT-503 showed no visible phenotype (Figure 3E). However, in cells with mitochondrial translation stress, dnSB inhibition in serine-less medium caused cell death (Figure 3E). Under PHGDH inhibition, medium-supplied serine alone was insufficient to compensate for dnSB loss. We confirmed this by tracing changes in D³-serine levels in medium and inside cells in response to mitochondrial translation inhibition with actinonin. Both treated and untreated cultures had a similar uptake capacity for serine (Figure S3G). These results emphasize that cells with mitochondrial translation stress depend on serine availability (Figure 3E). Because of such dramatic cell death under serine-deprived conditions (Figure S3H), we followed up all of our subsequent *in vitro* experiments in the presence of extracellular serine. Actinonin incubation only mildly affected cell viability after 24 h when assessed by markers of necrosis (propidium iodide) and apoptosis (Annexin V) and was not exacerbated by NCT-503 (Figure S3I). These data clearly demonstrated that mitochondrial dysfunction causes metabolic adaptation dependent on endogenous serine synthesis and proved *de novo* serine synthesis to be essential for cell survival under mitochondrial stress.

Next, we investigated how the metabolome is affected by serine deprivation. We first triggered short-term mitochondrial translation stress via actinonin (C2C12 cells) or genetic mutation

(E) Growth experiments under serine-containing and serine-deprived conditions in C2C12 myoblasts after 24 h of inhibition of mitochondrial translation (ACT) and/or dnSB (INH). Scale bar: 100 μ m. Differential interference contrast (DIC) imaging.

(F) Actinonin-treated (24 h) C2C12 myoblasts compared to untreated controls. Untargeted metabolomics.

(G) POLG^{D1135A} mutant overexpression (4 days) compared to POLG^{WT} expression. Untargeted metabolomics.

(H) Effect of short-term (2.5 h) inhibition of mitochondrial translation with or without NCT-503 compared to actinonin-only treated C2C12 cells. Untargeted metabolomics.

(I) Effect of *de novo* serine inhibition in POLG^{D1135A} mutant overexpression (4 days). Untargeted metabolomics.

(J) Mitochondrial oxidative stress upon inhibition of mitochondrial translation and/or dnSB. MitoSOX probe detection (cell borders are indicated with a white dotted line). Scale bar: 10 μ m.

(K) Mean MitoSOX intensity per cell from (J). Error bars represent SD.

(L) Mitochondrial membrane potential upon inhibition of mitochondrial translation (ACT) and/or dnSB (INH), tetramethylrhodamine methyl ester (TMRM) probe detection. Error bars represent SD.

(M) Mitochondrial and cytoplasmic translation products and ³⁵S-metabolic pulse labeling. Actinonin and NCT-503 treatments as in (E).

All metabolic data points represent the mean of biological quintuplicates of untargeted metabolomics; mRNA level from biological triplicates. Statistical significance was assessed using ANOVA. * $p \leq 0.05$, ** $p \leq 0.01$, *** $p \leq 0.001$. ACT, actinonin; DOX, doxycycline; PC, phosphatidylcholine; PE, phosphatidylethanolamine; PHGDH, D-3-phosphoglycerate dehydrogenase; PQ, paraquat; OM, oligomycin; ROT, rotenone; FCCP, p-trifluoro-methoxyphenyl hydrazone; TWNK, Twinkle; POLG, polymerase gamma.

(HEK cells overexpressing a POLG mutant). Both conditions showed increased serine levels with partially distinct lipid signatures and aspartate depletion (Figures 3F and 3G). When dnSB was inhibited in these mitochondrial stress conditions, phosphoserine decreased, and tricarboxylic acid cycle intermediates were altered (Figures 3H, 3I, S4A). The PE and PC lipid profile showed a decrease with dnSB inhibition alone, which was exacerbated at 6 h and partially recovered at 24 h with additional mitochondrial translation stress (Figure S3J). Interestingly, serine withdrawal alone caused an increase in oxidized GSH already at 2.5 h (Figure S4B). The intermediates of the *trans*-sulfuration pathway decreased, with a consequent decrease in GSH, impaired redox balance, and oxidative stress. Indeed, mitochondrial reactive oxygen species, assessed by MitoSOX signal, remarkably increased in cells with inhibition of both mitochondrial translation and dnSB but not with either treatment alone (Figures 3J and 3K). In addition, NCT-503 worsened the actinonin-induced mitochondrial respiration defect even when serine was supplemented in the medium (Figure S4C). This was also reflected in the loss of mitochondrial membrane potential (Figure 3L and S4D).

These results prompted us to assess translation capacity by ³⁵S-pulse labeling of *de novo* mitochondrial protein synthesis. The cells were pre-treated for 24 h (with or without actinonin and with or without serine) prior to the assay but were left in drug-free medium for the length of labeling. Actinonin, as expected, decreased mitochondrial translation rates with a rapid recovery when the drug was withdrawn. Strikingly, however, inhibition of *de novo* serine synthesis completely blocked the cellular ability to reinitiate mitochondrial protein synthesis (Figure 3M). Cytoplasmic translation capacity was unaffected by these treatments (Figure 3M). These data indicate that dnSB provides serine especially to mitochondria in stress to maintain mitochondrial translation.

To test the specificity of our findings with the NCT-503 inhibitor, we utilized additional non-serum stable pharmacological inhibitors of PHGDH with different modes of actions: CBR-5884, which prevents oligomerization of the enzyme,²⁵ and PKUMDL-WQ-2101,²⁶ which inhibits PHGDH via allosteric modifications. Both CBR-5884 and WQ-2101 triggered cell death strongest under mitochondrial stress when cells grew in medium depleted of serine (Figure S5A). The presence of extracellular serine partially mitigated this effect. PHGDH expression only mildly increased in response to its inhibitor alone in the presence or absence of serine in the medium (Figure S5B), while expression of ISR^{mt} transcriptional markers such as PSAT1, ATF4, and MTHFD2 was exacerbated by the lack of serine combined with mitochondrial translational stress (Figure S5B).

In summary, these data demonstrate that the non-essential amino acid serine becomes essential under a variety of conditions of mitochondrial stress. It maintains basic cellular functions, including lipid synthesis, and specifically supports translation of mtDNA-encoded proteins and keeps up oxidative functions.

DISCUSSION

Here, we report that serine becomes an essential amino acid in cells and tissues with mitochondrial translation stress. Our

data show that intracellular dnSB has a critical role in maintaining homeostasis in muscle with mitochondrial disease. In cultured cells with different kinds of mitochondrial dysfunction, dnSB is a first-line responder to mitochondrial stress. Remarkably, dnSB supports mitochondrial respiration and maintenance of the redox state, nucleotide homeostasis, and phospholipid pools. Inhibition of dnSB in MM mice aggravates histopathological and molecular hallmarks in skeletal muscle. Importantly, in mitochondrial RC deficiency, exogenous serine, which can be obtained from food or breakdown of proteins, is not able to compensate for the lack of dnSB. Our data indicate that a local supply of newly synthesized serine is essential to maintain mitochondrial translation and oxidative functions in tissues and cells with mitochondrial dysfunction.

The roles of serine as a regulator of stress responses are becoming increasingly clear.^{4–8} Serine is an important 1C donor for the folate-driven 1C cycle, the major anabolic pathway for cell growth and repair. The 1C cycle drives, e.g., GSH, nucleotide, and phospholipid synthesis and provides methyl units for epigenetic DNA or histone modifications. Its roles are crucial for rapidly growing cancer cells.^{14,15,27–31} Our data indicate that both postmitotic and proliferating cells with mitochondrial translation stress use similar, cancer cell-like anabolic pathways for restoration of cellular homeostasis. In a disease situation, serine drives essential repair and stress response pathways, including GSH synthesis, phospholipid synthesis, and maintenance of nucleotide homeostasis. Serine has also been suggested to be the limiting amino acid for mitochondrial translation.^{19,32} An essential role of dnSB may indeed be to secure the serine supply to sustain mitochondrial translation, probably both via serine-dependent formylation of the initiator methionine and by direct L-serine supply for translation.³³ Our results indicate that dysfunctional mitochondria become dependent on newly synthesized serine.

NCT-503 has not been found to cause major toxicity for healthy mice.^{15,34} This is surprising, as serine—in contrast to other amino acids—is directly used for synthesis of phosphatidylserine and ceramide species (the hydrophobic moiety of sphingolipids) that are important mediators of signaling cascades involved in apoptosis, proliferation, and stress responses.^{21,35} Blocking of dnSB or the extracellular serine supply has been reported to induce production of cytotoxic deoxy-sphingolipids and reduced ceramide pools but was not found to have an effect on total PC or PE pools in cultured cells.²¹ Our data indicate, however, that NCT-503 causes quite remarkable changes in phospholipid pools even in healthy aged mice, which is further aggravated by mitochondrial dysfunction.

In conclusion, our evidence highlights the importance of serine-directed pathways in maintenance of mitochondrial translation, oxidative functions, redox balance, and phospholipid synthesis in both growing cells and mitochondrial disease. Inhibition of *de novo* serine synthesis in mitochondrial dysfunction changes fuel utilization and modifies anabolic outputs of lipid synthesis and redox capacity in response to mitochondrial dysfunction. Our data indicate that mere serine supplementation cannot rescue the mitochondrial need for this amino acid in disease but approaches boosting *in situ* serine synthesis in

mitochondrial disease could attenuate disease progression. These findings indicate that the intracellular localization of serine biosynthesis is critical for survival under metabolic stress.

Limitations of the study

We targeted serine *de novo* synthesis *in vivo* using a single serum-stable inhibitor (NCT-503) and *in vitro* (NCT-503 and two other PHGDH inhibitors). While the effect on serine synthesis inhibition was confirmed with all three inhibitors *in vitro*, we cannot exclude the possibility that undetected *in vivo* off-target effects could exist for NCT-503. No signs of such effects were found in treated WT mice, which indicates that such effects would occur in a mitochondrial disease context. To study this, follow-up studies to validate new PHGDH inhibitors *in vivo* are required.

RESOURCE AVAILABILITY

Lead contact

Requests for further information, resources, and reagents should be directed to and will be fulfilled by the lead contact, Christopher B. Jackson (christopher.jackson@helsinki.fi).

Materials availability

All materials are available upon reasonable request from the [lead contact](#).

Data and code availability

- All data are available upon reasonable request from the [lead contact](#). Metabolomics data are provided as supplemental information.
- No original code has been generated for this study.
- Any additional information required to reanalyze the data reported in this paper is available from the [lead contact](#) upon request.

ACKNOWLEDGMENTS

The authors wish to thank Markus Innilä, Tuula Manninen, and Babette Hollmann for technical contributions and expertise and Prof. Johannes Spelbrink for provision of the T-REX HEK POLG and TWNK overexpressor cell lines. Open access funded by Helsinki University Library. The following funding sources are acknowledged: the Academy of Finland (A.S., decisions 207592, 303349, 361873, 345248; C.B.J., decision 336455), the Sigrid Jusélius Foundation (A.S.), the Swiss National Science Foundation (C.B.J., decision P2BEP3_162065), the Magnus Ehrnrooth Foundation (C.B.J.), the Novartis Foundation for Medical-Biological Research (C.B.J., decision 15A002), and the Henry Wellcome Fellowship (A.E.V., decision 215888/Z/19/Z).

AUTHOR CONTRIBUTIONS

Conceptualization, C.B.J., C.J.C., and A.S.; methodology, investigation, and formal analysis, C.B.J., A.M., T.M., R.A., G.M., N.Z., T.T., A.E.V., L.W., C.J.C., N.Z., N.A.K., and L.W.; supervision, C.B.J., C.J.C., and A.S.; funding acquisition, C.B.J. and A.S.; writing – original draft, C.B.J. and A.S.; writing – review & editing, all authors.

DECLARATION OF INTERESTS

The authors declare no competing interests.

STAR★METHODS

Detailed methods are provided in the online version of this paper and include the following:

- [KEY RESOURCES TABLE](#)
- [EXPERIMENTAL MODEL AND STUDY PARTICIPANT DETAILS](#)
 - Ethical approval

- Animal models

- Cell models

- [METHOD DETAILS](#)

- PHGDH inhibition in mice

- Cell culture and manipulations

- Cytoplasmic and mitochondrial translation labeling

- Mitochondrial isolation

- DNA manipulations and quantitation

- Gene expression

- Immunoblotting

- Microscopic structural analyses

- Immunofluorescent labeling of muscle tissue

- TMRM and mitoSOX stainings

- FACS analysis for cell cycle and viability

- Cell death assay

- Histological staining

- Targeted metabolomics

- Untargeted metabolomics

- Quantitative mass spectrometry of glycerophospholipids

- dNTP pool measurement

- Cell death count

- Oxymetric analyses

- [QUANTIFICATION AND STATISTICAL ANALYSIS](#)

SUPPLEMENTAL INFORMATION

Supplemental information can be found online at <https://doi.org/10.1016/j.celrep.2025.115710>.

Received: December 12, 2023

Revised: December 20, 2024

Accepted: April 25, 2025

Published: May 15, 2025

REFERENCES

1. Nunnari, J., and Suomalainen, A. (2012). Mitochondria: in sickness and in health. *Cell* 148, 1145–1159. <https://doi.org/10.1016/j.cell.2012.02.035>.
2. Vasan, K., Werner, M., and Chandel, N.S. (2020). Mitochondrial Metabolism as a Target for Cancer Therapy. *Cell Metab.* 32, 341–352. <https://doi.org/10.1016/j.cmet.2020.06.019>.
3. Gorman, G.S., Chinnery, P.F., Dimauro, S., Hirano, M., Koga, Y., McFarland, R., Suomalainen, A., Thorburn, D.R., Zeviani, M., and Turnbull, D. M. (2016). Mitochondrial diseases. *Nat. Rev. Dis. Primers* 2, 16080. <https://doi.org/10.1038/nrdp.2016.80>.
4. Forsström, S., Jackson, C.B., Carroll, C.J., Kuronen, M., Pirinen, E., Pradhan, S., Marmyleva, A., Auranen, M., Kleine, I.-M., Khan, N.A., et al. (2019). Fibroblast Growth Factor 21 Drives Dynamics of Local and Systemic Stress Responses in Mitochondrial Myopathy with mtDNA Deletions. *Cell Metab.* 30, 1040–1054.e7. <https://doi.org/10.1016/j.cmet.2019.08.019>.
5. Khan, N.A., Nikkanen, J., Yatsuga, S., Jackson, C., Wang, L., Pradhan, S., Kivelä, R., Pessia, A., Velagapudi, V., and Suomalainen, A. (2017). mTORC1 Regulates Mitochondrial Integrated Stress Response and Mitochondrial Myopathy Progression. *Cell Metab.* 26, 419–428.e5. <https://doi.org/10.1016/j.cmet.2017.07.007>.
6. Nikkanen, J., Forsström, S., Euro, L., Paetau, I., Kohnz, R.A., Wang, L., Chilov, D., Viinamäki, J., Roivainen, A., Marjamäki, P., et al. (2016). Mitochondrial DNA Replication Defects Disturb Cellular dNTP Pools and Remodel One-Carbon Metabolism. *Cell Metab.* 23, 635–648. <https://doi.org/10.1016/j.cmet.2016.01.019>.
7. Kühl, I., Miranda, M., Atanassov, I., Kuznetsova, I., Hinze, Y., Mourier, A., Filipovska, A., and Larsson, N.-G. (2017). Transcriptomic and proteomic landscape of mitochondrial dysfunction reveals secondary coenzyme Q deficiency in mammals. *Elife* 6, 1494. <https://doi.org/10.7554/elife.30952>.

8. Bao, X.R., Ong, S.-E., Goldberger, O., Peng, J., Sharma, R., Thompson, D. A., Vafai, S.B., Cox, A.G., Marutani, E., Ichinose, F., et al. (2016). Mitochondrial dysfunction remodels one - carbon metabolism in human cells. *Elife* 5, e10575. <https://doi.org/10.7554/elife.10575.001>.
9. Ignatenko, O., Nikkanen, J., Kononov, A., Zamboni, N., Ince-Dunn, G., and Suomalainen, A. (2020). Mitochondrial spongiotic brain disease: astrocytic stress and harmful rapamycin and ketosis effect. *Life Sci. Alliance* 3, e202000797. <https://doi.org/10.26508/lsa.202000797>.
10. Lehtonen, J.M., Forsström, S., Bottani, E., Viscomi, C., Baris, O.R., Iso-niemi, H., Höckerstedt, K., Österlund, P., Hurme, M., Jylhävä, J., et al. (2016). FGF21 is a biomarker for mitochondrial translation and mtDNA maintenance disorders. *Neurology* 87, 2290–2299. <https://doi.org/10.1212/wnl.0000000000003374>.
11. Pirinen, E., Auranen, M., Khan, N.A., Brilhante, V., Urho, N., Pessia, A., Hakkarainen, A., Kuula, J., Heinonen, U., Schmidt, M.S., et al. (2020). Niacin Cures Systemic NAD⁺ Deficiency and Improves Muscle Performance in Adult-Onset Mitochondrial Myopathy. *Cell Metab.* 31, 1078–1090.e5. <https://doi.org/10.1016/j.cmet.2020.04.008>.
12. Khan, N.A., Auranen, M., Paetau, I., Pirinen, E., Euro, L., Forsström, S., Pa-sila, L., Velagapudi, V., Carroll, C.J., Auwerx, J., and Suomalainen, A. (2014). Effective treatment of mitochondrial myopathy by nicotinamide riboside, a vitamin B3. *EMBO Mol. Med.* 6, 721–731. <https://doi.org/10.1002/emmm.201403943>.
13. Tynnismaa, H., Carroll, C.J., Raimundo, N., Ahola-Erkkilä, S., Wenz, T., Ruhanen, H., Guse, K., Hemminki, A., Peltola-Mjøsund, K.E., Tulkkii, V., et al. (2010). Mitochondrial myopathy induces a starvation-like response. *Hum. Mol. Genet.* 19, 3948–3958. <https://doi.org/10.1093/hmg/ddq310>.
14. Locasale, J.W., Grassian, A.R., Melman, T., Lyssiotis, C.A., Mattaini, K.R., Bass, A.J., Heffron, G., Metallo, C.M., Muranen, T., Sharfi, H., et al. (2011). Phosphoglycerate dehydrogenase diverts glycolytic flux and contributes to oncogenesis. *Nat. Genet.* 43, 869–874. <https://doi.org/10.1038/ng.890>.
15. Pacold, M.E., Brimacombe, K.R., Chan, S.H., Rohde, J.M., Lewis, C.A., Swier, L.J.Y.M., Possemato, R., Chen, W.W., Sullivan, L.B., Fiske, B.P., et al. (2016). A PHGDH inhibitor reveals coordination of serine synthesis and one-carbon unit fate. *Nat. Chem. Biol.* 12, 452–458. <https://doi.org/10.1038/nchembio.2070>.
16. Mehrmohamadi, M., Liu, X., Shestov, A.A., and Locasale, J.W. (2014). Characterization of the usage of the serine metabolic network in human cancer. *Cell Rep.* 9, 1507–1519. <https://doi.org/10.1016/j.celrep.2014.10.026>.
17. Possemato, R., Marks, K.M., Shaul, Y.D., Pacold, M.E., Kim, D., Birsoy, K., Sethumadhavan, S., Woo, H.-K., Jang, H.G., Jha, A.K., et al. (2011). Functional genomics reveal that the serine synthesis pathway is essential in breast cancer. *Nature* 476, 346–350. <https://doi.org/10.1038/nature10350>.
18. Vandekeere, S., Dubois, C., Kalucka, J., Sullivan, M.R., García-Caballero, M., Goveia, J., Chen, R., Diehl, F.F., Bar-Lev, L., Souffreau, J., et al. (2018). Serine Synthesis via PHGDH Is Essential for Heme Production in Endothelial Cells. *Cell Metab.* 28, 573–587.e13. <https://doi.org/10.1016/j.cmet.2018.06.009>.
19. Tajan, M., Hennequart, M., Cheung, E.C., Zani, F., Hock, A.K., Legrave, N., Maddocks, O.D.K., Ridgway, R.A., Athineos, D., Suárez-Bonnet, A., et al. (2021). Serine synthesis pathway inhibition cooperates with dietary serine and glycine limitation for cancer therapy. *Nat. Commun.* 12, 366. <https://doi.org/10.1038/s41467-020-20223-y>.
20. Mattaini, K.R., Sullivan, M.R., and Heiden, M.G.V. (2016). The importance of serine metabolism in cancer. *J Cell Biology* 214, 249–257. <https://doi.org/10.1083/jcb.201604085>.
21. Gao, X., Lee, K., Reid, M.A., Sanderson, S.M., Qiu, C., Li, S., Liu, J., and Locasale, J.W. (2018). Serine Availability Influences Mitochondrial Dynamics and Function through Lipid Metabolism. *Cell Rep.* 22, 3507–3520. <https://doi.org/10.1016/j.celrep.2018.03.017>.
22. Tynnismaa, H., Mjøsund, K.P., Wanrooij, S., Lappalainen, I., Ylikallio, E., Jalanko, A., Spelbrink, J.N., Paetau, A., and Suomalainen, A. (2005). Mutant mitochondrial helicase Twinkle causes multiple mtDNA deletions and a late-onset mitochondrial disease in mice. *Proc. Natl. Acad. Sci. USA* 102, 17687–17692. <https://doi.org/10.1073/pnas.0505551102>.
23. Besse, A., Wu, P., Bruni, F., Donti, T., Graham, B.H., Craigen, W.J., McFarland, R., Moretti, P., Lalani, S., Scott, K.L., et al. (2015). The GABA Transaminase, ABAT, Is Essential for Mitochondrial Nucleoside Metabolism. *Cell Metab.* 21, 417–427. <https://doi.org/10.1016/j.cmet.2015.02.008>.
24. Richter, U., Lahtinen, T., Marttinen, P., Myöhänen, M., Greco, D., Cannino, G., Jacobs, H.T., Lietzén, N., Nyman, T.A., and Battersby, B.J. (2013). A Mitochondrial Ribosomal and RNA Decay Pathway Blocks Cell Proliferation. *Curr. Biol.* 23, 535–541. <https://doi.org/10.1016/j.cub.2013.02.019>.
25. Mullarky, E., Lucki, N.C., Zavareh, R.B., Anglin, J.L., Gomes, A.P., Nicolay, B.N., Wong, J.C.Y., Christen, S., Takahashi, H., Singh, P.K., et al. (2016). Identification of a small molecule inhibitor of 3-phosphoglycerate dehydrogenase to target ser. *Proc. Natl. Acad. Sci. USA* 113, 1778–1783. <https://doi.org/10.1073/pnas.1521548113>.
26. Wang, Q., Liberti, M.V., Liu, P., Deng, X., Liu, Y., Locasale, J.W., and Lai, L. (2017). Rational Design of Selective Allosteric Inhibitors of PHGDH and Serine Synthesis with Anti-tumor Activity. *Cell Chem. Biol.* 24, 55–65. <https://doi.org/10.1016/j.chembiol.2016.11.013>.
27. Maddocks, O.D.K., Athineos, D., Cheung, E.C., Lee, P., Zhang, T., van den Broek, N.J.F., Mackay, G.M., Labuschagne, C.F., Gay, D., Kruiswijk, F., et al. (2017). Modulating the therapeutic response of tumours to dietary serine and glycine starvation. *Nature* 544, 372–376. <https://doi.org/10.1038/nature22056>.
28. Ngo, B., Kim, E., Osorio-Vasquez, V., Doll, S., Bustra, S., Liang, R.J., Luengo, A., Davidson, S.M., Ali, A., Ferraro, G.B., et al. (2020). Limited Environmental Serine and Glycine Confer Brain Metastasis Sensitivity to PHGDH Inhibition. *Cancer Discov.* 10, 1352–1373. <https://doi.org/10.1158/2159-8290.cd-19-1228>.
29. Muthusamy, T., Cordes, T., Handzlik, M.K., You, L., Lim, E.W., Gengatharan, J., Pinto, A.F.M., Badur, M.G., Kolar, M.J., Wallace, M., et al. (2020). Serine restriction alters sphingolipid diversity to constrain tumor growth. *Nature* 586, 790–795. <https://doi.org/10.1038/s41586-020-2609-x>.
30. Reid, M.A., Allen, A.E., Liu, S., Liberti, M.V., Liu, P., Liu, X., Dai, Z., Gao, X., Wang, Q., Liu, Y., et al. (2018). Serine synthesis through PHGDH coordinates nucleotide levels by maintaining central carbon metabolism. *Nat. Commun.* 9, 5442. <https://doi.org/10.1038/s41467-018-07868-6>.
31. Samanta, D., Park, Y., Andrabi, S.A., Shelton, L.M., Gilkes, D.M., and Semenza, G.L. (2016). PHGDH Expression Is Required for Mitochondrial Redox Homeostasis, Breast Cancer Stem Cell Maintenance, and Lung Metastasis. *Cancer Res.* 76, 4430–4442. <https://doi.org/10.1158/0008-5472.can-16-0530>.
32. Sullivan, M.R., Mattaini, K.R., Dennstedt, E.A., Nguyen, A.A., Sivanand, S., Reilly, M.F., Meeth, K., Muir, A., Darnell, A.M., Bosenberg, M.W., et al. (2019). Increased Serine Synthesis Provides an Advantage for Tumors Arising in Tissues Where Serine Levels Are Limiting. *Cell Metab.* 29, 1410–1421.e4. <https://doi.org/10.1016/j.cmet.2019.02.015>.
33. Kory, N., Wyant, G.A., Prakash, G., Uit de Bos, J., Bottanelli, F., Pacold, M. E., Chan, S.H., Lewis, C.A., Wang, T., Keys, H.R., et al. (2018). SFXN1 is a mitochondrial serine transporter required for one-carbon metabolism. *Science* 362, eaat9528. <https://doi.org/10.1126/science.aat9528>.
34. Padrón-Barthe, L., Villalba-Orero, M., Gómez-Salineró, J.M., Acín-Pérez, R., Cogliati, S., López-Olañeta, M., Ortiz-Sánchez, P., Bonzón-Kulichenko, E., Vázquez, J., García-Pavía, P., et al. (2018). Activation of Serine One-Carbon Metabolism by Calcineurin A β 1 Reduces Myocardial Hypertrophy and Improves Ventricular Function. *J. Am. Coll. Cardiol.* 71, 654–667. <https://doi.org/10.1016/j.jacc.2017.11.067>.
35. Kay, J.G., and Fair, G.D. (2019). Distribution, dynamics and functional roles of phosphatidylserine within the cell. *Cell Commun. Signal* 17, 126. <https://doi.org/10.1186/s12964-019-0438-z>.
36. Robinson, B.H., Petrova-Benedict, R., Buncic, J.R., and Wallace, D.C. (1992). Nonviability of cells with oxidative defects in galactose

- medium: a screening test for affected patient fibroblasts. *Biochem. Med. Metab. Biol.* **48**, 122–126.
37. Birsoy, K., Wang, T., Chen, W.W., Freinkman, E., Abu-Remaileh, M., and Sabatini, D.M. (2015). An Essential Role of the Mitochondrial Electron Transport Chain in Cell Proliferation Is to Enable Aspartate Synthesis. *Cell* **162**, 540–551. <https://doi.org/10.1016/j.cell.2015.07.016>.
 38. King, M.P., and Attardi, G. (1989). Human Cells Lacking mtDNA: Repopulation with Exogenous Mitochondria by Complementation. *Science* **246**, 500–503. <https://doi.org/10.1126/science.2814477>.
 39. Löffler, M., Jöckel, J., Schuster, G., and Becker, C. (1997). Dihydroorotat-ubiquinone oxidoreductase links mitochondria in the biosynthesis of pyrimidine nucleotides. *Mol. Cell. Biochem.* **174**, 125–129.
 40. Rygiel, K.A., Grady, J.P., Taylor, R.W., Tuppen, H.A.L., and Turnbull, D.M. (2015). Triplex real-time PCR—an improved method to detect a wide spectrum of mitochondrial DNA deletions in single cells. *Sci. Rep.* **5**, 9906. <https://doi.org/10.1038/srep09906>.
 41. Jackson, C.B., Gallati, S., and Schaller, A. (2012). qPCR-based mitochondrial DNA quantification: Influence of template DNA fragmentation on accuracy. *Biochem. Biophys. Res. Commun.* **423**, 441–447. <https://doi.org/10.1016/j.bbrc.2012.05.121>.
 42. Rocha, M.C., Grady, J.P., Grünewald, A., Vincent, A., Dobson, P.F., Taylor, R.W., Turnbull, D.M., and Rygiel, K.A. (2015). A novel immunofluorescent assay to investigate oxidative phosphorylation deficiency in mitochondrial myopathy: understanding mechanisms and improving diagnosis. *Sci Rep* **5**, 15037. <https://doi.org/10.1038/srep15037>.
 43. Ahmed, S.T., Alston, C.L., Hopton, S., He, L., Hargreaves, I.P., Falkous, G., Oláhová, M., McFarland, R., Turnbull, D.M., Rocha, M.C., and Taylor, R.W. (2017). Using a quantitative quadruple immunofluorescent assay to diagnose isolated mitochondrial Complex I deficiency. *Sci. Rep.* **7**, 15676. <https://doi.org/10.1038/s41598-017-14623-2>.
 44. Fuhrer, T., Heer, D., Begemann, B., and Zamboni, N. (2011). High-Throughput, Accurate Mass Metabolome Profiling of Cellular Extracts by Flow Injection–Time-of-Flight Mass Spectrometry. *Anal. Chem.* **83**, 7074–7080. <https://doi.org/10.1021/ac201267k>.
 45. Xia, J., Psychogios, N., Young, N., and Wishart, D.S. (2009). MetaboAnalyst: a web server for metabolomic data analysis and interpretation. *Nucleic Acids Res.* **37**, W652–W660. <https://doi.org/10.1093/nar/gkp356>.
 46. Tatsuta, T. (2017). Quantitative Analysis of Glycerophospholipids in Mitochondria by Mass Spectrometry. *Methods Mol. Biol.* **1567**, 79–103. https://doi.org/10.1007/978-1-4939-6824-4_7.
 47. Özbalci, C., Sachsenheimer, T., and Brügger, B. (2013). Membrane Biogenesis, Methods and Protocols. *Methods Mol Biology* **1033**, 3–20. https://doi.org/10.1007/978-1-62703-487-6_1.

STAR★METHODS

KEY RESOURCES TABLE

REAGENT or RESOURCE	SOURCE	IDENTIFIER
Antibodies		
Chicken anti-MTHFD2	Abcam	Cat# ab37840; RRID:AB_776544
Rabbit anti-phospho-eIF2a	Abcam	Cat# ab32157; RRID:AB_732117
Rabbit anti-eIF2a	Cell Signaling Technology	Cat# 9722; RRID:AB_2230924
Rabbit anti-GRP75 (HSP70)	Abcam	Cat# ab53098; RRID:AB_880311
Mouse anti-Opa1	BD Transduction Laboratories	Cat# 612606; RRID:AB_399888
Rabbit anti-SFXN1	Sigma	Cat# HPA019543; RRID:AB_1856789
Rabbit anti-S6 p(240/244)	Cell Signaling	Cat# 2215S; RRID:AB_331682
Rabbit anti-S6	Cell Signaling	Cat# 2217; RRID:AB_331355
Goat anti-ATF4	Abcam	Cat# ab1371; RRID:AB_300588
Rabbit anti-PHGDH	Proteintech	Cat# 14719-1-AP; RRID:AB_2283938
Mouse anti-beta-Actin	Cell Signaling	Cat# 3700S; RRID:AB_2242334
Rabbit anti-Porin/VDAC1	Abcam	Cat# ab15895; RRID:AB_2214787
Rabbit anti-TOM20	Santa Cruz	Cat# sc-11415; RRID:AB_2207533
Mouse anti-MTCO1	Abcam	Cat# ab14705; RRID:AB_2084810
Mouse anti-SDHA	Abcam	Cat# ab14715; RRID:AB_301433
Rabbit anti-Laminin	Sigma Aldrich	Cat# L9393; RRID:AB_477163
Goat anti-Rabbit, HRP conjugated	Molecular Probes	Cat# G21234; RRID:AB_1500696
Goat Anti-Mouse, HRP conjugated	Jackson ImmunoResearch	Cat# 115-035-146; RRID:AB_2307392
Goat Anti-Mouse IgG2a, Alexa 488	Thermo Fisher Scientific	Cat# A21131; RRID:AB_2535771
Goat anti-Mouse IgG1, biotin conjugated	Thermo Fisher Scientific	Cat# A10519; RRID:AB_1500809
Goat anti-Rat IgG (H + L), Alexa 488	Thermo Fisher Scientific	Cat# A11006; RRID:AB_2534074
Chemicals, peptides, and recombinant proteins		
NCT-503	Sigma Aldrich	Cat# SML1659
CBR-5884	MedChem Express	Cat# HY-100012
PKUMDL-WQ-2101	MedChem Express	Cat# HY-123269
Actinonin	Sigma Aldrich	Cat# A6671
Paraquat	Sigma Aldrich	Cat# 36541
Oligomycin	Sigma Aldrich	Cat# O4876
FCCP	Sigma Aldrich	Cat# C2920
Antimycin A	Sigma Aldrich	Cat# A8674
Rotenone	Sigma Aldrich	Cat# R8875
MEM	Gibco	Cat# 11095
DMEM w/out Met and Cys	Sigma Aldrich	Cat# D0422
Glutamax	Thermo Fisher Scientific	Cat# 35050038
Fetal Bovine Serum (FBS) Heat Inactivated	Sigma Aldrich	Cat# F9665
Fetal Bovine Serum (FSC) dialyzed	Thermo Fisher Scientific	Cat# A3382001
Sodium pyruvate	Thermo Fisher Scientific	Cat# 11360039
L-Serine	Sigma Aldrich	Cat# S4311
D3-Serine	Cambridge Isotope Laboratories	Cat# DLM-582-0.1
EasyTag Express 35S protein labeling mix	PerkinElmer	Cat# NEG772014MC
Anisomycin	Sigma Aldrich	Cat# A9789
Chloramphenicol	Sigma Aldrich	Cat# C3175
Pierce™ Protease Inhibitor Tablets, EDTA-free	Thermo Fisher Scientific	Cat# A32955

(Continued on next page)

Continued

REAGENT or RESOURCE	SOURCE	IDENTIFIER
Halt™ Phosphatase Inhibitor Cocktail	Thermo Fisher Scientific	Cat# PI78420
TRIzol	Thermo Fisher Scientific	Cat# 15596018
SYBR Green Supermix	Bio Rad	Cat# 1725006CUST
Protein Assay Dye Reagent Concentrate	Bio Rad	Cat# 500-0006
VECTASHIELD® Antifade Mounting Medium, With DAPI	Vector Laboratories	Cat# H-1200-10
Streptavidin Alexa 647	Life Technologies	Cat# S32357
Image-iT™ TMRM Reagent	Thermo Fisher Scientific	Cat# I34361
Aqueous Glutaraldehyde EM Grade 25%	Electron Microscopy Sciences	Cat# 16210
Poly(ethylene glycol) BioUltra, 4000	Sigma Aldrich	Cat# 95904
(2-Hydroxypropyl)-beta-cyclodextrin	Sigma Aldrich	Cat# H107-5G
EDTA	Sigma Aldrich	Cat# E9884
Dimethyl sulfoxide (DMSO)	Sigma Aldrich	Cat# D8418
ProLong™ Gold Antifade Mountant	Thermo Fisher Scientific	Cat# P36934

Critical commercial assays

miRNeasy Micro kit	Qiagen	Cat# 217004
Maxima First Strand cDNA Synthesis Kit for RT-qPCR	Thermo Fisher Scientific	Cat# K1672
MitoTracker® Red CMXRos	Thermo Fisher Scientific	Cat# M-7512
MitoSOX Red Mitochondrial Superoxide Indicator	Thermo Fisher Scientific	Cat# M36008
SYTOX™ Green Dead Cell Stain	Thermo Fisher Scientific	Cat# S34860
Vector Shield Avidin-Biotin blocking kit	Vector laboratories	Cat# SP-2001
Vector Shield Mouse on Mouse (MOM) blocking kit	Vector laboratories	Cat# MKB-2213

Experimental models: Cell lines

C2C12 mouse myoblast	ATCC	CRL-1772
Human diploid male control myoblast (established in-lab)	Suomalainen Lab	N/A
Flp-In™ T-REX™ 293 POLG and TWNK mutants	Spelbrink Lab	N/A

Experimental models: Organisms/strains

Tg/ACTB/twnk-p.353-365-dup/BL6	Suomalainen Lab	N/A
--------------------------------	-----------------	-----

Oligonucleotides

SCL7A11 mouse Fwd: 5'- CATATGCTGGCTGGTTTTACCTC -3'	Metabion	N/A
SCL7A11 mouse Rev: 5'- CACGTTTGTTCAGTACGTAGCCC -3'	Metabion	N/A
Psat1 mouse Fwd: 5'- AGTGGAGCGCCAGAATAGAA -3'	Metabion	N/A
Psat1 mouse Rev: 5'- CTTGCGTTGTGACAGCGTTA -3'	Metabion	N/A
Phgdh mouse Fwd: 5'- GACCCCATCATCTCTCCTGA -3'	Metabion	N/A
Phgdh mouse Rev: 5'- GCACACCTTTCTTGCCTGA -3'	Metabion	N/A
β-Actin mouse Fwd: 5'- ATGCTCCCGGGCTGTAT -3'	Metabion	N/A
β-Actin mouse Rev: 5'- CATAGGAGTCCTTCTGACCCATTC -3'	Metabion	N/A
Trib3 mouse Fwd: 5'- TCGCTTTGTCTTCAGCAACTGTGAG -3'	Metabion	N/A
Trib3 mouse Rev: 5'- CATCAGCCGCTTTGCCAGAGTAG -3'	Metabion	N/A
Mthfd2 mouse Fwd: 5'- CATGGGGCATATGGGAGATAAT -3'	Metabion	N/A

(Continued on next page)

Continued

REAGENT or RESOURCE	SOURCE	IDENTIFIER
Mthfd2 mouse Rev: 5'- CCGGGCCGTTTCGTGAGC -3'	Metabion	N/A
Gdf15 mouse Fwd: 5'- CAACCAGAGCCGAGAGGAC -3'	Metabion	N/A
Gdf15 mouse Rev: 5'- TGCACGCGGTAGGCTTC -3'	Metabion	N/A
Fgf21 mouse Fwd: 5'- ACCTGGAGATCAGGGAGGAT -3'	Metabion	N/A
Fgf21 mouse Rev: 5'- GCACAGGAACCTGGATGTCT -3'	Metabion	N/A
Atrogin-1 (F box32) mouse Fwd: 5'- CTCTGTACCATGCCGTTCCCT -3'	Metabion	N/A
Atrogin-1 (F box32) mouse Rev: 5'- GGCTGCTGAACAGATTCTCC -3'	Metabion	N/A
MuRF-1 (Trim63) mouse Fwd: 5'- ACCGAGTGCAGACGATCATC -3'	Metabion	N/A
MuRF-1 (Trim63) mouse Rev: 5'- TGGCGTAGAGGGTGCAAAC -3'	Metabion	N/A
mtDNA triplex (ND4) Fwd: 5'- CCATTCTCCTCCTATCCCTCAAC -3'	Metabion	N/A
mtDNA triplex (ND4) Rev: 5'- CACAATCTGATGTTTTGGTTAAACTATATT -3'	Metabion	N/A
mtDNA triplex (ND4) Probe: 5'-6FAM-CCGACATCATTACCGGGTTTTCTCTTG -3'	Metabion	N/A
mtDNA triplex (D Loop) Fwd: 5'- CCCACACGTTCCCCTTAAATAA -3'	Metabion	N/A
mtDNA triplex (D Loop) Rev: 5'- CGTGAGTGGTTAATAGGGTGATAGAC -3'	Metabion	N/A
mtDNA triplex (D Loop) Probe: 5'- ROX-ACATCACGATGGATCAC -3'	Metabion	N/A
18S mouse Fwd: 5'- CGGACAGGATTGACAGATTG -3'	Metabion	N/A
18S mouse Rev: 5'- CAAATCGCTCCACCAACTAA -3'	Metabion	N/A
Mt-Rnr1 mouse Fwd: 5'- AGGAGCCTGTTCTATAATCGATAAA -3'	Metabion	N/A
Mt-Rnr1 mouse Rev: 5'- GATGGCGGTATATAGGCCGAA -3'	Metabion	N/A

Software and algorithms

Image Lab	Bio Rad	https://www.bio-rad.com/en-fi/product/image-lab-software
Prism 6	GraphPad	https://www.graphpad.com/
ImageJ/FIJI	N/A	https://fiji.sc/
FlowJo v10	Biosciences	https://www.flowjo.com/solutions/flowjo
iTEM	Olympus	https://www.olympus-sis.com
Photoshop v23.5.1	Adobe	https://www.adobe.com
MetaboAnalyst 3.0	MetaboAnalyst	https://www.metaboanalyst.ca/
LipidView v.1.2	SCIEX	https://sciex.com/products/software/lipidview-software

Other

Mouse diet	Altromin	Cat# C1000
------------	----------	------------

EXPERIMENTAL MODEL AND STUDY PARTICIPANT DETAILS

Ethical approval

The National Animal Experiment Review Board and Regional State Administrative Agency for Southern Finland approved the animal experimentation, which were conducted according to the European Union Directive. Maintenance of mice was performed under licences: ESAVI/11682/04.10.07/0217.

Animal models

The Deletor mice express a dominant in-frame duplication, homologous to a human progressive external ophthalmoplegia (PEO) mutation. Deletor mice were used as an *in vivo* model system of mitochondrial dysfunction. Deletors ubiquitously overexpress mitochondrial Twinkle helicase carrying a human patient mutation. Due to the mtDNA replication defect, these animals accumulate mtDNA deletions which lead to late onset muscle myopathy.²² Two previously reported transgene lines were used in this study.²² The lines differ by severity of the disease: D line showing a stronger myopathy phenotype as compared to the C line. Age- and sex-matching wild type animals were used as controls.

Cell models

The primary myoblasts line used was isolated from a healthy 45-years-old male Caucasian donor as described before.⁵ The mouse myoblast cell line C2C12 (CRL-1772) was obtained authenticated from ATCC. The Flp-In T-REx 293 POLG and TWNK mutants were obtained from the Spelbrink lab. All cell lines were routinely tested for mycoplasma infection.

METHOD DETAILS

PHGDH inhibition in mice

Daily injections of the vehicle and the compound were performed intraperitoneally to 24-months-old male mice. Treatment length of 30 days. NCT-503 was freshly prepared prior to the injections. 20 μ M stock was dissolved in EtOH (5%), PEG400 (35%) and 30% Cyclodextrin (60%) and was administered to the mice at serum-stable concentrations of 40 mg/kg.¹⁵

Cell culture and manipulations

Mammalian cells with mitochondrial RC dysfunction are metabolically dependent on glycolysis to source ATP,³⁶ on pyruvate for aspartate synthesis³⁷ and pyrimidines³⁸ and uridine.³⁹ Therefore, all experimental conditions contained glucose, pyruvate and uridine as indicated.

Murine C2C12 myoblast cells were grown in MEM (Gibco, 11095) with or without L-serine (Sigma, S4311; 42.0 mg/L). Culturing of primary diploid human myoblasts was performed as described before.⁵ If not indicated otherwise, cells were treated in 150 μ M actinonin for indicated time points \pm NCT-503 and \pm Serine. Inhibitor treatments were done for indicated time points: 100 μ M Paraquat (Sigma, 36541), 2 μ g/mL oligomycin (Sigma, O4876), 10 μ M FCCP (Sigma, C2920), 2 μ g/mL antimycin A (Sigma, A8674), 1 μ M rotenone (Sigma, R8875) for indicated time point were applied. Growth curves for cumulative differences in growth under actinonin treatment was performed over 72 h and values plotted as the cumulative population doubling as follows:

$$\text{Population doubling} = (\log(\text{cell number Day 3}) - \log(\text{cell number Day 0})) / \log(2)$$

Cytoplasmic and mitochondrial translation labeling

Mitochondrial translation assays were performed with EasyTag Express ³⁵S protein labeling mix (PerkinElmer, #NEG772014MC). Assays were performed in cells grown on 60 mm dishes, pretreated with drugs for 24 h. Cells were incubated for 30 min in 2 mL of pre-warmed media consisting of DMEM without methionine or cysteine (Sigma #D0422) supplemented with 1x glutamax, 10% dialyzed FBS and 1 mM sodium pyruvate. To inhibit cytoplasmic translation anisomycin (Sigma #A9789) was added to the cells to a final concentration of 100 μ g/mL 5 min prior to the addition of the EasyTag labeling mix. For cytoplasmic labeling, chloramphenicol (40 μ g/mL) was added 30 min prior to labeling. For pulse labeling cells were washed, incubated with the labeling mix and harvested after 30 min. Protein extracts were separated on 12% stain-free polyacrylamide gels (Bio-Rad), the gels were dried and exposed to a phosphor imaging screen. Phosphor imaging screens were imaged using an FLA-7000 Typhoon scanner (GE Healthcare) and total protein was imaged using a Chemidoc imaging system (Bio-Rad).

Mitochondrial isolation

Mitochondria were isolated from quadriceps femoris (QF) from Deletors to enrich for mitochondrial protein. Briefly, QF was homogenized in a Potter-Elvehjem with a rotor-driven pestle in HIM buffer (10 mM HEPES-KoH, pH7.6, 100 mM KCl, 3 mM MgCl₂, 0.1 mM EDTA, 10% glycerol) supplemented with 1 mM PMSF and protease inhibitors (Sigma). Briefly, one-half of the QF was lysed in 5 mL HIM buffer, strained with a 100 μ m-pore cell strainer and the sieve rewashed with 5 mL homogenization buffer. Mitochondrial fractions were obtained by differential centrifugation at a low step at 700xg for 20 min and resulting supernatant at 10'000xg and was repeated. All steps were performed at 4°C.

DNA manipulations and quantitation

Total genomic DNA was extracted by proteinase K digestion following standard phenol–chloroform extraction with ethanol precipitation or column-based extraction (Macherey–Nagel). MtDNA deletion load was assessed with a modified triplex assay by measuring D Loop, ND1 and ND4 simultaneously.^{5,40} MtDNA copy number was determined by real-time quantitative PCR (qPCR) as described before^{5,41} with primers indicated in the [key resources table](#). All RT–qPCR measurements were performed on a CFX96 Touch qPCR system (Biorad) using IQ SybrGreen kit (Biorad) as previously described.⁴ Primers sequences are available ([key resources table](#)).

Gene expression

RNA was extracted by standard TRIzol (Invitrogen) chloroform precipitation from snap-frozen tissues homogenized by a Fast-Prep w-24 Lysing Matrix D (MP Biomedical) and Precellys w-24 (Bertin Technologies) apparatus. Total RNA from cells was extracted using a miRNeasy kit (Qiagen) according to the manufacturer's instructions. DNase digestion was either in eluted RNA or on-column. Usually, 2 µg of total RNA was reverse transcribed using the Maxima first strand cDNA synthesis kit (ThermoFisher). Quantitative real-time PCR amplification of cDNA was performed with IQ SybrGreen kit (Biorad) on CFX96 Touch qPCR system (Biorad). Relative expressions were normalized to β-actin or 18S rRNA. The linear range and specificity of all primer pairs was determined by serial dilutions and sequencing.

Immunoblotting

Total protein was extracted with RIPA buffer using phosphatase inhibitors tablets (ThermoFisher Scientific) and sodium orthovanadate to preserve phosphorylation sites. Protein extracts from tissue were prepared as described.⁴ Briefly, tissues were homogenized in 1xPBS containing Triton X- and dodecyl maltoside (f.c.1%) in a Precellys w-24 bead homogenizer (Bertin Technologies), incubated on ice for 30 min and collected by centrifugation at 20'000xg for 20 min. Protein concentrations were determined using Bradford assay. Proteins were separated on appropriate gels by SDS-PAGE usually on 4–20% gradient gels (Biorad), transferred to PVDF membranes and blocked with 5% milk in 1xTBS-T for 1 h and primary antibodies incubated overnight at 4°C in 1:1000 in 3% BSA in TBS-T buffer. Antibodies used were: MTHFD2 (Abcam, #ab37840), SDHA (Abcam, ab14715), p-S6 (Cell signaling, #4858), total S6 (Cell signaling, #2217), and β-ACTIN (Santa Cruz, #1616), TOM20 (Santa Cruz, #11415), PORIN/VDAC1 (Abcam, #ab15895), HSP70 (Abcam, #ab53098), α-TUBULIN (Abcam, #28439), Eif2α (Invitrogen, #4478G), PHGDH (Proteintech, #14719-1-AP), EIF2S1 (p-S51) ab32157, SFXN1 (Sigma, # HPA019543).

Microscopic structural analyses

Mitochondrial staining was performed as described before.⁴ Briefly, the cells were stained for 15 min in 50 nM Mitotracker CMXRos, rinsed with 1xPBS and fixed in ice-cold acetone and mounted in VectaShield. Immunohistochemistry and immunofluorescence staining were performed as described before.⁴ Samples were imaged in a Zeiss Observer 2.1 equipped with ApoTome technology. Image contrast was adjusted within the software of the microscope. For electron microscopy samples were fixed in 2% glutaraldehyde in phosphate buffer and routinely processed. Contrast enhancement was performed using ITEM software and Photo-shop 23.5.1.

Immunofluorescent labeling of muscle tissue

Mitochondrial immunofluorescent labeling was performed using a protocol adapted from.⁴² Briefly, 10 µm cryosections were thawed at room temperature for 1 h, before fixing for 3 min in 4% PFA. Sections were washed, and then permeabilised using an ascending and descending methanol gradient (70% for 10 min, 95% for 10 min, 100% for 20 min, 95% for 10 min and 70% for 10 min). Sections were washed with TBST and blocked with 10% NGS for 1h. Following further TBST washes sections were blocked using a Vector Shield Avadin-Biotin blocking kit. Sections were blocked with Avidin D solution for 15 min and Biotin solution for 15 min, with TBST washes after each. Sections were then blocked with a Vector Shield Mouse on Mouse (MOM) blocking kit following the manufacturer's instructions. Anti-Mt-Co1 (Abcam ab14705, 1:100), anti-SDHA (Abcam ab14715, 1:100) and anti-Laminin (Sigma-Aldrich L9393, 1:50) were diluted in MOM dilutant and applied to sections before incubation overnight at 4°C. The next day sections were washed with TBST and secondary antibodies Goat Anti-mouse IgG2a Alexa 488 (Life Technologies A21131, 1:200) and Goat anti-Mouse IgG1 biotin (Life Technologies A10519, 1:200) were diluted in MOM dilutant and applied to sections before incubating for 2h at 4°C. Sections were washed with TBST and then Streptavidin Alexa 647 (Life Technologies S32357, 1:100) and DAPI (1:400) were diluted in MOM dilutant and applied to the sections before incubation 2h at 4°C. Sections were washed and mounted in prolong Gold antifade mountant before imaging.

Serial sections to those used for mitochondrial labeling were labeled for p-S6. Briefly, sections were thawed at room temperature for 1 h, before fixing with methanol free 4% PFA for 15 min. Slides were rinsed in PBS and sections blocked with 1xPBS/5% NGS/0.3% Triton for 1 h at room temperature. Sections were blocked with an Avidin-Biotin blocking kit as described above. Antibodies p-S6 (Cell Signaling, #4858, 1:100) were diluted in 1xPBS/1%BSA/0.3%Triton and incubated overnight at 4°C. Following washes, secondary antibody Goat anti-Rabbit Alexa 488 (Life Technologies A11006, 1:200), was diluted in 1xPBS/1%BSA/0.3%Triton, and applied to sections before incubation for 2 h at 4°C. Sections were washed before mounting in prolong Gold and imaging.

Imaging of both experiments was completed using an AxioImager Z1 with motorised stage and sections were tiled using Zen Blue edition. For the mitochondrial section single muscle fibers were segmented automatically using an inhouse software as described

previous.⁴³ This allowed us to export an average intensity for mtco1 and SDHA and muscle fiber area. The number of central nuclei were counted and expressed as a percentage of the total fibers analyzed. For the p-S6 section fibers were manually segmented in the same software to export mean p-S6 intensity per fiber. Comparison of serial sections allowed us to assess the levels of pS6 at a single cell level in the context of mitochondrial MT-CO1 and SDHA.

TMRM and mitoSOX stainings

To measure mitochondrial membrane potential tetramethylrhodamine methyl ester (TMRM) probe (Sigma-Aldrich) was used. Reactive oxygen species were assayed using MitoSox (Thermo Fisher Scientific). Cells were stained 30 min with TMRM or 15 min for MitoSOX. FCCP was used as positive control. Cells were washed with 1xPBS and imaged in phenol red free medium using an Evos microscope system. Quantitation was performed using ImageJ.

FACS analysis for cell cycle and viability

Cell cycle and apoptosis were assayed using propidium iodide (PI) with subsequent FACS sorting. Apoptosis was assayed using a combined PI and AnnexinV staining following the manufacturer's instructions. All cells were sampled at 24 h incubation with the indicated concentrations, if not mentioned otherwise. Samples were run on a BD Science Accuri FACS machine. Subsequent data analysis and image generation was performed using FlowJo.

Cell death assay

The rate of cell death was evaluated by using a Sytox Green Dead Cell stain (S34860, Thermo Scientific). The staining was used according to the manufacturer's instructions. All measurements and quantifications were performed with IncuCyte S3.

Histological staining

Histological stainings for COX/SDH were performed as described.^{4,6}

Targeted metabolomics

Targeted metabolomic analysis was performed as before.⁴ Briefly, 20 mg of tissue was homogenised in a Precellys w-24 (Bertin Technologies) apparatus with added 20 μ L of internal labeled standard mix and 500 μ L of pure acetonitrile (ACN) and 1% formic acid (FA) with second step extraction of 500 μ L of 90/10% ACN/H₂O+1%FA.

To assess serine flux, cells were cultured in serine-less media with labeled D3-serine ((98%; DLM-582-0.1, Cambridge Isotope Laboratories) or unlabelled L-serine at a final concentration of 285 μ M for 6 h and media and cells collected. Cells were washed once in 1xPBS and metabolites extracted by direct scraping in a precalculated volume of ice-cold methanol/ACN/H₂O. All samples were analyzed and quantified using WATERS XEVO-TQ-S triple quadrupole mass spectrometer coupled to ultra-pressure liquid chromatography.

Untargeted metabolomics

Untargeted analysis and cold metabolome extraction was applied for metabolomics from cells. Briefly, cells were grown on 6-well dishes and collected by washing twice in 75 mM ammonium citrate buffer (pH 7.4) and immediately flash frozen in liquid nitrogen. Samples were extracted by extraction buffer (ACN:methanol:water) at -20° C and analyzed as described before.⁴⁴ Muscle tissue samples were subjected to a hot extraction protocol. Briefly, approximately 20 mg of snap-frozen tissue were homogenised in 500 μ L 70% (v/v) ethanol in water (extraction solvent) in a pre-cooled Precellys w-24 (Bertin Technologies) apparatus with the use of ceramic beads. Lysed sample was transferred to a 15 mL tube with an additional wash with 500 μ L extraction solvent for a total of 1 mL. During these steps, samples were kept at -20° C in an ethanol cold bath at all times. Hot extraction was performed by addition of 75° C warm extraction solvent to the lysed samples and incubated for 1 min. After extraction, samples were cooled to -20° for storage. For analysis, samples were vacuum-dried, resuspended in water prior to analysis. Extracted samples were analyzed on an Agilent 6550 QTOF instrument in negative mode. Putative annotations were created by matching to Human Metabolome Database v.3.6. using mass per charge (0.001 m/z tolerance) and isotopic correlation patterns.

Untargeted and targeted data was analyzed using MetaboAnalyst 3.0 software in interquartile range, autoscaled, log-transformed and missing values estimated by KNN.⁴⁵ Testing between groups was performed using univariate analyses, multiple t-testing and two-way ANOVA. Separation was tested in unsupervised multivariate, partial least squares discriminant (PLSDA) analysis. Metabolites from targeted metabolomics were rated significant if $p \leq 0.05$.

Quantitative mass spectrometry of glycerophospholipids

Mass-spectrometric analysis was performed essentially as described.^{46,47} Lipids were extracted from mitochondria-enriched fraction in the presence of internal standards of major phospholipids (PC 17:0-20:4, PE 17:0-20:4, PI 17:0-20:4, PS 17:0-20:4, PG 17:0-20:4, PA 17:0-20:4, all from Avanti Polar Lipids) and CL (CL mix I, Avanti Polar Lipids). Extraction was performed according to Bligh and Dyer with modifications and analyzed on a QTRAP 6500 triple quadrupole mass spectrometer (SCIEX) equipped with nano-infusion spray device (TriVersa NanoMate with ESI-Chip type A, Advion). Mass spectra were processed by the LipidView Software Version 1.2 (SCIEX) for identification and quantification of lipids. Lipid amounts (pmol) were corrected for response differences

between internal standards and endogenous lipids. Correction of isotopic overlap in CL species was performed as described previously.⁴⁶

dNTP pool measurement

dNTP pool measurement was done as previously described before.⁶

Cell death count

Representative images for each condition were captured and three non-overlapping fields of view (320 μm^2 each) randomly selected per image for quantification ($n = 6-9$ per condition). Cells were categorized based on total cell number and the number of dead cells. Cell death was quantified as the percentage of dead cells relative to the total cell count.

Oxymetric analyses

Oxygen consumption rates were measured using a high-resolution oxygraph (OROBOROS instruments using a substrate-uncoupler-inhibitor protocol. Specific oxygen consumption rates are expressed as $\text{pmol}/(\text{s}\cdot\text{mg})$. Briefly, 2×10^6 cells were resuspended in respiration buffer (0.5 mM EGTA, 3 mM MgCl_2 , 60 mM Lactobionic acid, 20 mM Taurine, 10 mM KH_2PO_4 , 20 mM HEPES, 110 mM D-Sucrose, 1% fat-free BSA). Oxygen consumption rates were performed in the presence of pyruvate-glutamate-malate and activities determined with +ADP (CI), +succinate (CI + CII), maximal uncoupled respiration by FCCP titration and CIV by ascorbate +TMPD.

QUANTIFICATION AND STATISTICAL ANALYSIS

Statistical analysis data are presented as the means \pm SEM for animal experiments and \pm SD for cellular assays, if not stated otherwise. Unless stated otherwise statistical significance was calculated using unpaired Statistical significance was determined using one-way ANOVA for mouse groups or Student's t test and represented in GraphPad Prism 8.4.1. with $*p \leq 0.05$, $**p \leq 0.01$, $***p \leq 0.001$. In each figure sample size, repetitions and statistical test are indicated. For false positive analysis of targeted metabolomics, the Benjamini-Hochberg method with a critical value of 0.2 was used.